Efficient Red Organic Light Emitting Diodes of Nona Coordinate Europium Tris(β-diketonato) Complexes Bearing 4'-Phenyl-2,2':6',2''-terpyridine

Dr. Rashid Ilmi,*[a] Jingyu Wang,[b] Dr. José D. L. Dutra,[c] Prof. Dr. Liang Zhou,*[b] Prof. Dr. Wai-Yeung Wong,*[d] Prof. Dr. Paul R. Raithby*[e], and Prof. Dr. Muhammad S. Khan*[a]

[a]Department of Chemistry, Sultan Qaboos University, P. O. Box 36, Al Khod 123, Oman

[b]State Key Laboratory of Rare Earth Resource Utilization, Changchun Institute of Applied Chemistry, Chinese Academy of Sciences, Renmin Street 5625, Changchun 130022, People's Republic of China.

[c]Pople Computational Chemistry Laboratory, Department of Chemistry, UFS, 49100-000 São Cristóvão, Sergipe, Brazil.

[d]Department of Applied Biology and Chemical Technology and Research Institute for Smart Energy, The Hong Kong Polytechnic University, Hung Hom, Kowloon, Hong Kong, People's Republic of China.

[e]Department of Chemistry, University of Bath, Claverton Down, Bath, BA2 7AY, UK

E-mail addresses and ORCID ID of corresponding authors:

Rashid Ilmi (RI) : rashidilmi@gmail.com; 0000-0002-5165-5977

Liang Zhou (LZ) : zhoul@ciac.ac.cn; 0000-0002-2751-5974

Wai-Yeung Wong (WYW) : wai-yeung.wong@polyu.edu.hk; 0000-0002-9949-7525

Paul R. Raithby : p.r.raithby@bath.ac.uk; 0000-0002-2944-0662

Muhammad S. Khan (MSK) : msk@squ.edu.om; 0000-0001-5606-6832

Abstract: Two novel nona coordinate ternary Eu(III) β-diketonate complexes i.e., [Eu(β-diketonate)$_3$(Ph-TerPyr)], β-diketonate = 4,4,4-trifluoro-1-phenyl-1,3-butanedione (btfa) (**Eu-1**) and 4,4,4-trifluoro-1-(2-naphthyl)-1,3-butanedione (NTA) (**Eu-2**)] and Ph-TerPyr = 4'-phenyl-2,2':6',2''-terpyridine have been synthesized and characterized. The structure of the complexes was elucidated by density functional theory (DFT) methods. Shape analysis further revealed that the coordination geometry around Eu(III) ion distorted spherical tricapped trigonal prism (D_{3h}) and distorted spherical capped square antiprism (C_{4v}) for **Eu-1** and **Eu-2**, respectively. The experimental photophysical properties of the complexes were investigated and complemented with theoretical calculations. Effective energy transfer (ET) pathway for the sensitized red luminescence is discussed. The complexes were tested as emitting layer (EML) in OLEDs. Ten OLEDs (five single-EML and five double-EML) were fabricated for each complex by vacuum thermal evaporation method. At the optimum doping concentration of 4 wt%, the double-EML OLEDs of **Eu-1** exhibited red electroluminescence (EL) with an EQE of 4.0% and maximum brightness (B) = 1179 cd/m^2, maximum current efficiency (η_c) = 5.64 cd/A, maximum power efficiency (η_p) = 4.78 lm/W with very low turn-on voltage ($V_{turn\text{-}on}$) = 3.6 V at the current density (J) of 10 mA/cm^2. Interestingly, the double-EML OLEDs of **Eu-2** at the optimum concentration of 3 wt%, displayed an outstanding EL performance with EQE of 7.32% and B = 838 cd/m^2, η_c = 10.19 cd/A, η_p = 10.33 lm/W, and $V_{turn\text{-}on}$ = 3.1 V at J =10 mA/cm^2. The EL performance of this device is among the best reported for devices incorporating a europium complex as a red emitter.

Keywords: β-diketone; Europium(III); Sensitized Luminescence; Electroluminescence

Introduction

The sensitized red emission of Eu(III) ion by organic ligands in their neutral organo-europium complexes (OEuCs) has been researched and manoeuvred intelligently to develop interesting functional materials such as organic light emitting diodes (OLEDs)[1], sensors,[2] sensitizers to improve OLED performance of red-emitting Ir(III) complex[3], and temperature sensing[4]. Among the many types of OEuCs, arguably tris(β-diketonato)Eu(III) complexes comprising polydentate ancillary ligand(s) have been extensively explored and utilized in different applications, especially OLEDs. Interestingly, a search in the literature revealed that the most dominant complexes in this class are octa coordinated and reports on the nine coordinate OEuCs are relatively limited. However, it is important to emphasize that nine coordinate complexes[5] with different tridentate ligand(s) have been reported exhibiting large photoluminescence quantum yield (PLQY = 71%) with ultralong observed luminescence lifetime (τ_{obs} = 2.94 ms)[6]. These could be excellent candidates for sensing and biological applications but may not be good for OLEDs since longer excited state lifetime leads to low efficiency of OLEDs. On the other hand, neutral tris(β-diketonate) complexes comprising different ancillary ligands (*N^N*/*O^O*/*N^N^N*/*O^O^O* etc) displayed large PLQY despite their relatively short τ_{obs} for Eu($^5D_0$), which implies shorter natural radiative lifetime (τ_{rad}) and thus could be beneficial for generating good EL performance.[7] In other words, shortening of the τ_{rad} means that forbidden 4f – 4f electronic transitions become more allowed. According to the Judd-Ofelt (J-O) theory,[8] the forbidden 4f–4f electronic transitions become partially allowed when the symmetry of the coordination sphere around Ln(III) is reduced and is directly related to the orbital mixing between 4f and 5d.[9] Recently, we have employed an asymmetric, large bite angle *N^N* ligand [2-(2-pyridyl)benzimidazole; Py-Im] and symmetrical β-diketone (hexafluoroacetylacetone; hfaa) generating a new octa coordinate [Eu(hfaa)$_3$Py-Im] complex with an uncommon distorted trigonal dodecahedral (D_{2d} with continuous shape measure value (CshM = 0.745) coordination geometry around Eu(III).[3a] The complex displayed large

PLQY and fairly good EL properties. To further improve the photophysical as well as EL properties, we replaced the symmetric hfaa by an asymmetric btfa ligand generating another [Eu(btfa)$_3$Py-Im] complex.[1c] Replacement of symmetrical by asymmetrical ligand further distorted the coordination geometry ([Eu(btfa)$_3$Py-Im]; CshM = 0.997) resulting in more allowed transition that led to further shortening of the τ_{obs} and thus the OLEDs based on [Eu(btfa)$_3$Py-Im] delivered improved EL performance compared to [Eu(hfaa)$_3$Py-Im] and analogues.

It is well-known that the nona coordinated complexes are more asymmetric than octa coordinated complexes and thus we would speculate the complexes to have more allowed 4f electronic transitions leading to shorter τ_{obs}. Generally, the coordination geometry of luminescent lanthanide complexes comprising β-diketonate and tridentate ancillary ligands are mostly spherical capped square antiprism (C_{4v})[10] and tricapped trigonal prism (D_{3h})[11], which are lower symmetry than the coordination geometry of octa coordinated complexes (distorted square antiprism/trigonal dodecahedral)[12]. Learning from our own experiences as well as from the literature, in the present work, we have utilized a simple tridentate terpyridine ancillary ligand, Ph-TerPyr to develop new asymmetric OEuCs of general formula [Eu(β-diketonate)$_3$(Ph-TerPyr)] [β-diketonate = btfa (**Eu-1**) and NTA (**Eu-2**), **Fig. 1**] bearing asymmetrical btfa and NTA. Terpyridine is a classic rigid, planar neutral tridentate chelating ligand playing a pivotal role in the development of coordination chemistry.[13] The complexes are characterized and the photophysical properties are assessed and discussed. The roles of ligands in sensitizing **Eu-1** and **Eu-2** emission are evaluated and discussed with the help of experimental results and theoretical methods using DFT and time-dependent density functional theory (TD-DFT). Furthermore, with the help of obtained data and LUMPAC,[14] the energy migration processes involved are elucidated and discussed for the complexes. It is interesting to emphasize and to our surprise, most of the [Eu(β-diketonate)$_3$(Terpyridine)] complexes reported so far in the literature are utilized as sensors [2a-c] or molecular machines and logic gates[15] while reports on the EL are rare except a polymer light

emitting diode by Yang et al.,[16] with B = 68.2 cd/m^2 with a very high $V_{turn\text{-}on}$ = 17 V. In continuation of our commitment to improve the EL performance of red-emitting OEuCs and the given scarcity of EL data, we further employed the complexes as EML to fabricate OLEDs and subsequently analysed and discussed their EL performance.

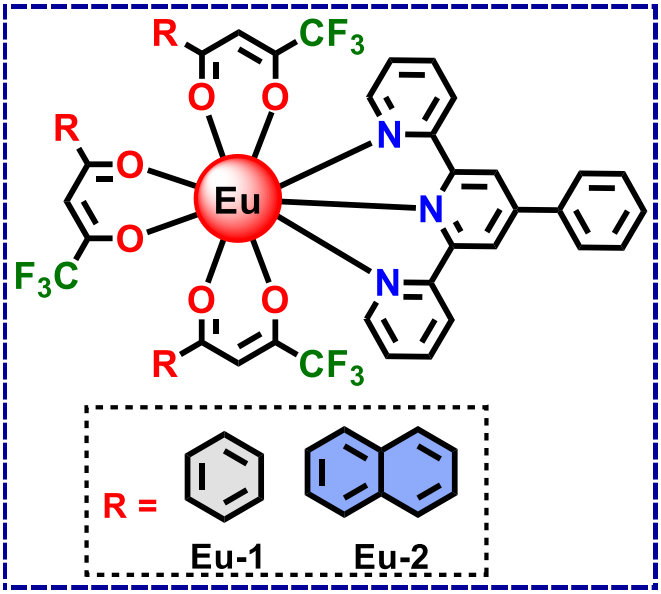

Figure 1: Chemical structures of new nonacoordinate OEuCs.

Results and Discussion:

The new OEuCs were synthesized by the method reported earlier[7] and characterized by elemental analysis, mass spectrometry, FT-IR spectroscopy and thermogravimetric analysis (**Figs. S1 – S5, ESI**). The results of these studies attest to the formulation of **Eu-1** and **Eu-2** as [Eu(btfa)$_3$(Ph-TerPyr)] and [Eu(NTA)$_3$(Ph-TerPyr)], respectively. Repeated attempts to grow single crystal for structure determination were not rewarding; however, as noted by us[1c, 7, 12a] and others[17], structural information obtained through DFT calculations have the same degree of accuracy as determined by the single crystal X-ray diffraction (SC-XRD) with an overall root mean square deviation (RMSD) value of the coordination sphere as low as 0.17 Å.[12a] Moreover, theoretical calculations of the photophysical properties depend on the modelling of the ground state geometry of the studied complex. **Fig. 2** shows the ground state geometry of the **Eu-1** and **Eu-2** complexes optimized at the PBE1PBE/TZVP/MWB52 level of theory. To elucidate the

ground state geometry of the complexes, the crystallographic coordinates of an analogous complex (CSD code KIBKEM [18]) were utilized (details are included in Section 1.1.1 of ESI). The spherical coordinate of each atom directly coordinated to the central Eu(III) ion is shown in **Table S1, ESI**. It is observed that the average Eu-O bond distances for both complexes are around 2.43 Å, which is shorter than the respective average Eu–N (2.65 Å) distance. It was noted by us[1a] that the average Eu-N bond distance for complexes containing the Eu(III) ion calculated applying different DFT methods was marginally longer than the Eu-N bond distances determined experimentally. Furthermore, a comparison between the experimental and theoretical structure in terms of RMSD considering all atoms of the complex/atoms of the coordination polyhedra further revealed that the DFT method provides geometries in accordance with those obtained by the SC-XRD. These data were further considered to calculate important photophysical properties and energy migration pathways for the sensitized luminescence. The data obtained were further employed to calculate the shape and symmetry of the coordination sphere by utilizing SHAPE program.[19] The polyhedral geometry of the Eu(III) ion has a nona coordination environment composed of six oxygen (O) donors from the primary β-diketone ligands and three nitrogen (N) donors of the Ph-TerPy ligands (N_3O_6), as can be seen in **Fig. 2**. The DFT result in conjunction with SHAPE program further revealed that **Eu-1** polyhedron is a distorted spherical tricapped trigonal prism, with D_{3h} symmetry around the Eu(III) ion (**Table S2, ESI**). The same analysis for **Eu-2** reveals that the coordination polyhedron is better described as a distorted spherical capped square antiprism, with polyhedron geometrical symmetry idealized as C_{4v}. As expected, the geometry of **Eu-2** is more asymmetric than **Eu-1,** since the order of the C_{4v} point group (8 symmetry operations) is lower than the order of D_{3h} (12 symmetry operations). This could be attributed to the bulkier i.e., naphthyl group of the β-diketonate ligands in **Eu-2**.

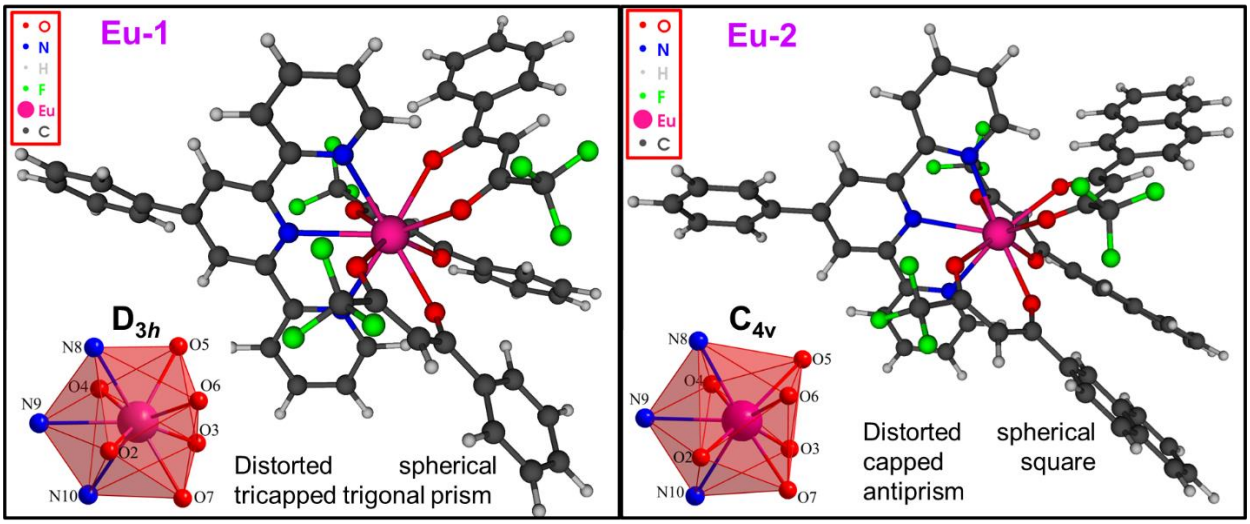

Figure 2: Geometry of **Eu-1** and **Eu-2** complexes calculated at the PBE1PBE/TZVP/MWB52 level of theory.

Analysis and discussion of experimental and theoretical photophysical properties

The absorption spectra of the complexes and free Ph-TerPy recorded in dilute CH_2Cl_2 solution (1×10^{-5} M) are shown in **Fig. 3a**. The spectra of the complexes displayed combined absorption of the ligands (β-diketone and Ph-TerPy) with λ_{max}^{abs} = 325 nm, molar absorptivity (ε) 14,053 $M^{-1}cm^{-1}$ for **Eu-1** while **Eu-2** displayed two strong absorptions at λ_{max}^{abs} = 267 nm (ε ≈ 15,800 $M^{-1}cm^{-1}$) and 335 nm (ε ≈ 12,387 $M^{-1}cm^{-1}$). The high ε for both complexes suggests that the complexes have strong light absorbing capability and thus strong emitting complexes could be realized. Moreover, the absorption spectrum of **Eu-2** exhibits a redshift of 21 nm compared to **Eu-1** due to enhanced conjugation.

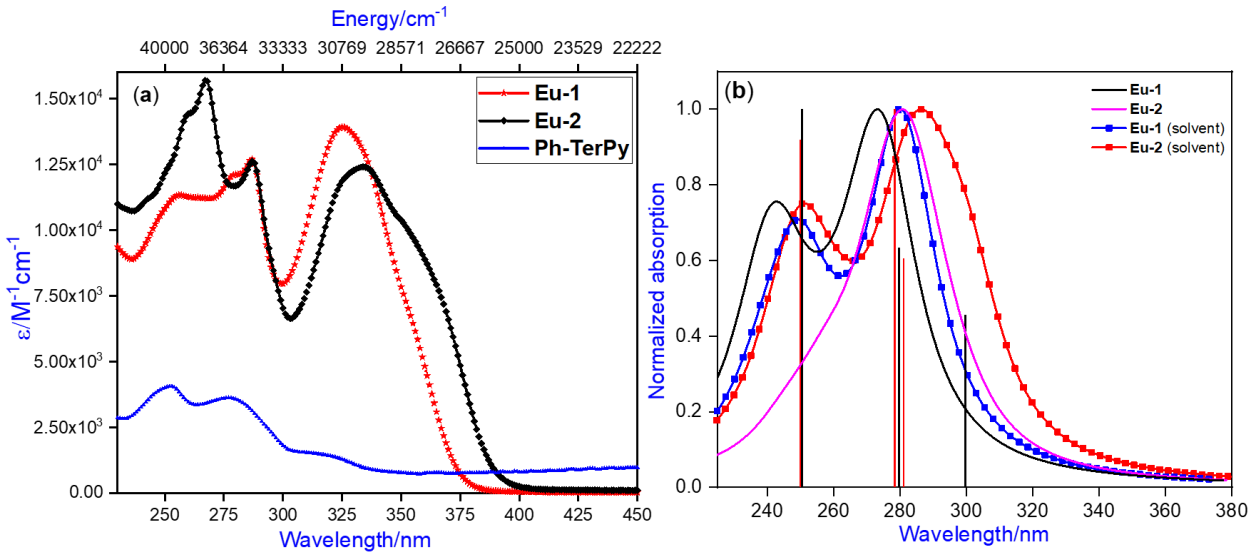

Figure 3: (a) Absorption spectra of **Eu-1**, **Eu-2** and free Ph-TerPy in CH_2Cl_2. (b) Theoretical absorption spectra predicted by the TD-DFT method (with and without the implicit effect of solvent) for **Eu-1** and **Eu-2** from the geometry calculated at the PBE1PBE/TZVP/MBW52 level of theory.

To understand the experimental optical absorption spectroscopy results clearly and the involvement of the ligands (β-diketone and Ph-TerPy) in the light absorption phenomenon, we employed the TD-DFT method to predict the theoretical absorption spectra. As can be seen from **Fig. 3(b),** λ_{max}^{abs} value is slightly underestimated in both cases i.e., with or without solvent. Such behaviour was also observed previously by us [1a] and by others[20], where theoretical absorption spectra obtained by the TD-DFT method using different density functionals were marginally underestimated. Qualitatively, the effect of the solvent resulted in more agreement of the spectra with those observed experimentally. It was noted that the theoretical absorption spectrum of **Eu-2** displays a higher absorbance value in lower wavelength regions similar to the experimental result. To further understand the origin of transitions, we performed the natural transition orbitals (NTOs) at CAM-B3LYP/TZVP/MWB52 level of theory for the three most intense singlet (S) excited states. The NTO analysis provides a simple portrayal of the transition density between the ground and the excited state. [21] The analysis indicates that the most intense bands of both complexes

are derived from the electronic transitions involving MOs centred both in the β-diketonate and Ph-TerPy ligands (**Fig. 4**). Moreover, it further reveals that lower wavelength transition originated from the neutral Ph-TerPy, which is supported by the experimental absorption spectrum of Ph-TerPy. On the other hand, the absorption bands more displaced towards the longer wavelength region predominantly rely on the participation of electronic transitions from the MOs centred on β-diketonate ligands.

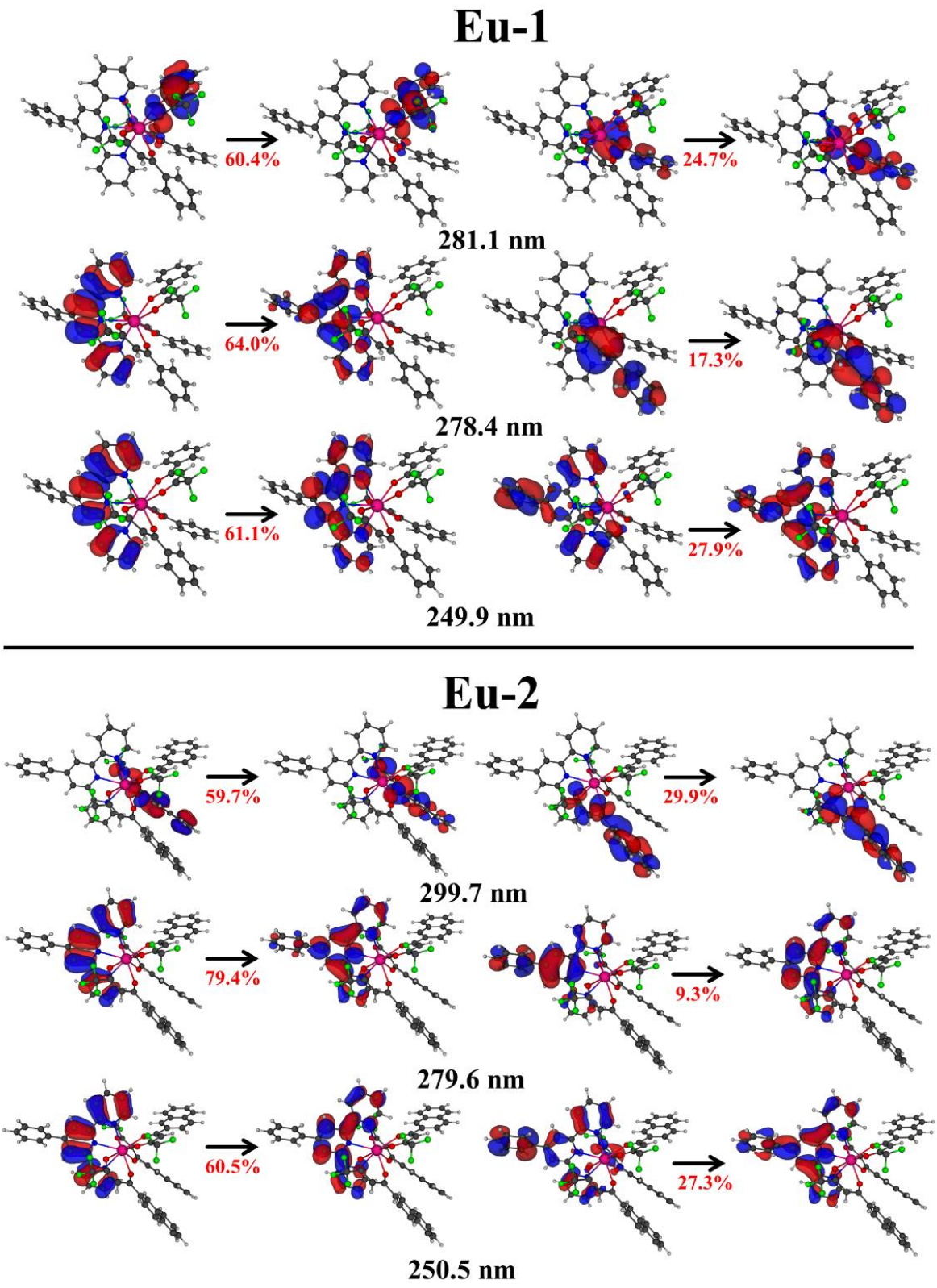

Figure 4: Picture of the NTO mainly contributing to the most intense bands of **Eu-1** and **Eu-2** calculated with CAM-B3LYP/TZVP/MWB52 (DCM), where the percentages indicate the contribution of the main NTO for each transition.

Fig. 5 shows the PL spectra of the complexes in the solid-state by exciting them at their λ_{max}^{abs}. The spectra exhibit typical well-resolved europium centred emission in the region between 400 and 750 nm. The excitation spectra display prominent ligand bands in the UV range and faint f–f transitions at 463 nm ($^5D_2 \leftarrow {}^7F_{0,4}$) and 533 nm ($^5D_{1,2} \leftarrow {}^7F_{1,4}$) for **Eu-1** and untraceable transitions for **Eu-2**, thus confirming the sensitisation of the europium PL by the antenna mechanism[12b, 22] (overlapping absorption, excitation and PL spectra is shown **Figs. S6 - S9, ESI**). Important emission data extracted from the PL spectra such as the barycentre of the transitions, emission intensity of the transitions and % contribution of each transition relative to magnetic-dipole $^5D_0 \rightarrow {}^7F_1$ transition is listed in **Table 1**.

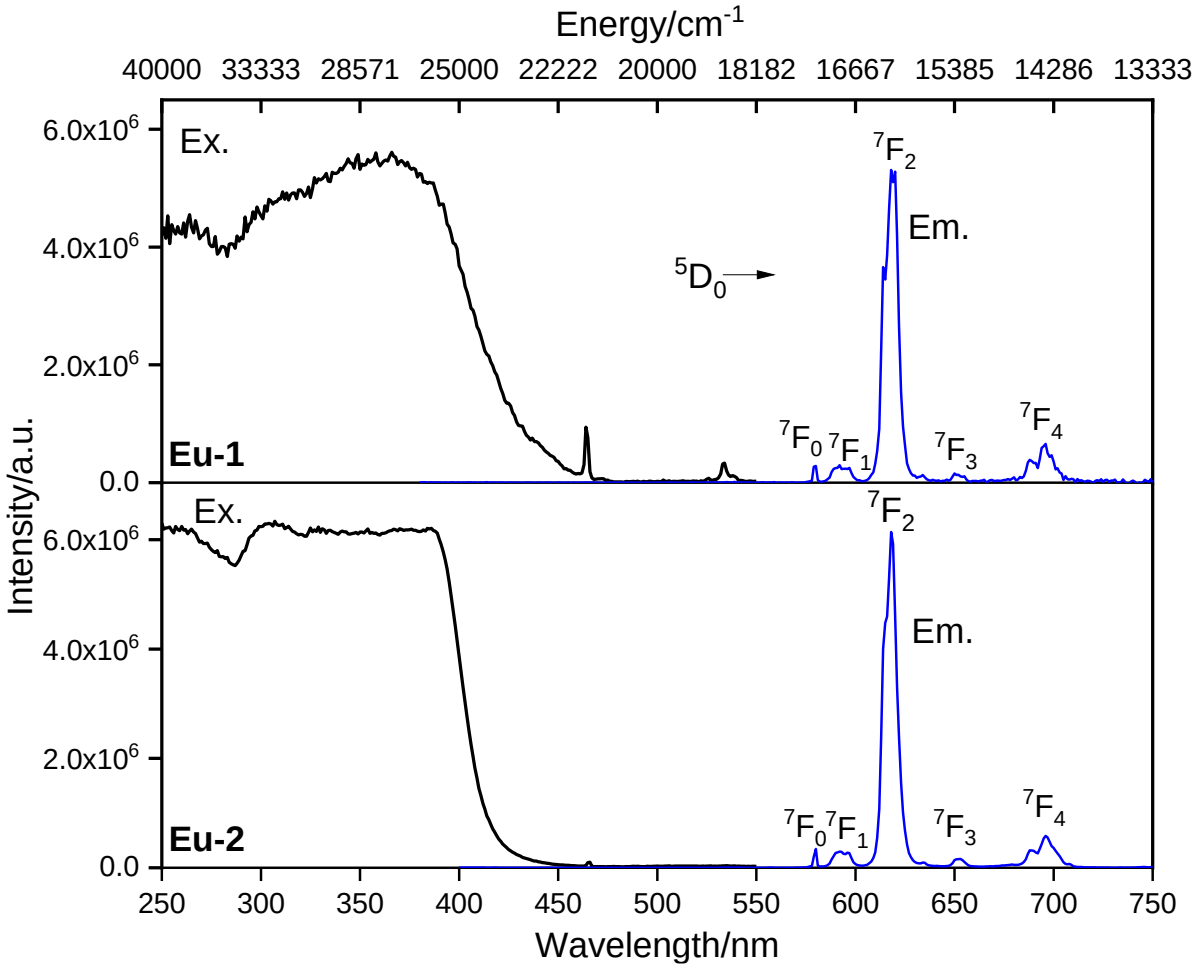

Figure 5: Excitation and emission spectra of **Eu-1** and **Eu-2** in the solid-state at room temperature.

The PL spectrum in each case is dominated by the induced electric-dipole ($^5D_0 \rightarrow {}^7F_2$) transition which comprises 78.38 and 80.41% (**Table 1**) total integrated intensity relative to magnetic-dipole transition $^5D_0 \rightarrow {}^7F_1$ for **Eu-1** and **Eu-2**, respectively (**Fig. 5**). This is responsible for brilliant red emission with the CIE colour coordinates (x = 0.671; y = 0.325)$_{\textbf{Eu-1}}$ **(Fig. S10, ESI)** and (x = 0.675; y = 0.323)$_{\textbf{Eu-2}}$ **(Fig. S11, ESI)**, which is almost identical to the standard red colour recommended by NTSC (0.67, 0.33) and thus could serve as a red component to manufacture white-OLEDs by RGB method. The higher relative intensity of the $^5D_0 \rightarrow {}^7F_2$ with respect to $^5D_0 \rightarrow {}^7F_1$ i.e. R_{21} implies that Eu(III) is coordinated in a site without an inversion centre and symmetry around the Eu(III) ion is lower, which indeed is the case as determined by the continuous shape measures (CShMs). As expected, the R_{21} of **Eu-2** (18.81) is higher than **Eu-1** (15.74) and could be associated with a more asymmetric coordination sphere in the case of **Eu-2** (C_{4v}). Furthermore, the higher integral intensity $^5D_0 \rightarrow {}^7F_2$ transitions over the $^5D_0 \rightarrow {}^7F_1$ transition points towards the dominance of forced electric dipole (FED) and dynamic coupling (DC) mechanism in the emission process of these complexes.[23]

To establish and clearly understand the photophysics, we further determined the excited lifetime (τ_{obs}) of the $^5D_0$ emitting state in the solid-state. The τ_{obs} was calculated by the fitting of the PL decay curve (**Figs. S12 & S13, ESI**) as displayed in **Figs. S14 & S15, ESI** and data obtained are gathered in **Table 1**. The decay profiles in each case reveal mono-exponential fitting and confirm the presence of single major emitting species. Both the complexes displayed fairly long lifetime with the τ_{obs} = 600.15 ± 2.14 μs (χ^2 = 1.004) and 449 ± 1.01 μs (χ^2 = 1.028) for **Eu-1** and **Eu-2**, respectively. The complexes exhibit large PLQY in the solid-state with Q_{Eu}^{L} = 54.90 and 44.95% for **Eu-1** and **Eu-2**, respectively, which is higher than reported nona coordinated Eu(III) analogues.[2a, 2d, 24] Moreover, shorter τ_{obs} values and higher Q_{Eu}^{L} values of the present complexes than highly asymmetric octa coordinated trigonal dodecahedral (D_{2d})

[Eu(btfa)$_3$Py-Im] (τ_{obs} = 660 µs and Q_{Eu}^{L} = 40.8%)[1c] and [Eu(hfaa)$_3$Py-Im] (τ_{obs} = 833.01µs and Q_{Eu}^{L} = 33.0%)[3a] suggest that the forbidden 4f–4f electronic transitions are more allowed and the orbital mixing between 4f and 5d is higher in the present complexes.

Table 1: Experimental and theoretical photophysical properties of **Eu-1** and **Eu-2** in the solid-state.

Photophysical Parameters	**Eu-1**	**Eu-2**
$^5D_0 \rightarrow {}^7F_0$	17260.21 cm^{-1} (0.22;1.09 %)[a]	17254.27 cm^{-1} (0.22; 0.94%)[a]
$^5D_0 \rightarrow {}^7F_1$	16862.19 cm^{-1}	16860.38 cm^{-1}
$^5D_0 \rightarrow {}^7F_2$	16174.79 cm^{-1} (15.74; 78.38%)[a]	16176.50 cm^{-1} (18.81; 80.41%)[a]
$^5D_0 \rightarrow {}^7F_3$	15306.62 cm^{-1} (0.43; 2.73 %)[a]	15331.51 cm^{-1} (0.43; 1.83%)[a]
$^5D_0 \rightarrow {}^7F_4$	14384.2 cm^{-1} (2.69; 13.40 %)[a]	14406.39 cm^{-1} (2.93; 12.52 %)[a]
FWHM of $^5D_0 \rightarrow {}^7F_2$	8.76 nm	7.83 nm
Intensity Ratio (R_{21})[b]	15.74	18.81
CIE Color Coordinates	x= 0.671; y = 0.325	x= 0.675; y = 0.323
τ_{obs} (µs)	600.15 ± 2.14 µs (χ^2 = 1.004)	449± 1.01 µs (χ^2 = 1.028)
Ω_2 (× 10^{-20} cm^2)[c]	27.91 [27.90]	33.32 [33.33]
Ω_4 (× 10^{-20} cm^2)[c]	10.61 [10.62]	11.50 [11.50]
A_{Rad} (s^{-1})[d]	1066.35 [1047.55]	1240.38 [1223.77]
A_{NRad} (s^{-1})[e]	600.31 [618.70]	986.79 [1003.40]
τ_R (µs)[f]	937.77	806.20
Q_{Eu}^{Eu} (%)[g]	63.98 [62.9]	55.69 [55.0]
Q_{Eu}^{L} (%)	54.90 [55.8]	44.95 [44.4]
η_{Sen} (%)[g]	85.80 [88.9]	80.71 [80.8]

Values in the square parentheses are calculated theoretically; [a](Emission transition intensities;% intensity of each transitions relative to magnetic-diploe $^5D_0 \rightarrow {}^7F_1$ transition); [b]Ratio of the electric-dipole transitions ($^5D_0 \rightarrow {}^7F_2$) to magnetic-dipole transition ($^5D_0 \rightarrow {}^7F_1$) i.e., $R_{21} = I(^5D_0 \rightarrow {}^7F_2) \Big/ I(^5D_0 \rightarrow {}^7F_1)$

[c]calculated using Eq. 1; [d]calculated using Eq. 2 and Eq. 3; [e]calculated using Eq. 4; [f]calculated using Eq. 5; [g]calculated using Eq. 6; [h]calculated using Eq. 7

To understand the results more clearly, we have further determined the A_{Rad} and A_{NRad} by utilizing the steady-state PL spectra and τ_{obs} with the help of the set of equations 2 – 4. As can be seen from **Table 1**, both the complexes displayed large value of A_{Rad} = 1066.35 s^{-1} for **Eu-1** and A_{Rad} = 1240.38 s^{-1} for **Eu-2**. The larger A_{Rad} in the case **Eu-2** implies that the extent of mixing of 4f-5d orbitals is higher in **Eu-2** and thus made intrinsic parity-forbidden 4f-4f transition more allowed leading to faster i.e., shortening of the Eu($^5D_0$) radiative lifetime. It is well established that to produce faster Eu(III) radiation rates one needs to design anti-symmetrical Eu(III) complexes with larger value of Ω_2 parameter.[25] In particular, Ω_2 is more sensitive to the symmetry and sequence of ligand fields. Interestingly, both complexes displayed large value of the Ω_2 (**Table 1**). As expected, the Ω_2 = 33.32 × 10^{-20} cm^2 value for **Eu-2** is higher than that of **Eu-1** (Ω_2 = 27.91 × 10^{-20} cm^2). This is due to the lower symmetry C_{4v} of **Eu-2** than **Eu-1** (D_{3h}) and fits very well with the predictions made from group theoretical considerations.[26]

Theoretical understanding of the energy transfer mechanism

To understand the ET processes of the sensitized luminescence[27] of the present complexes clearly, energy of the lowest singlet (S_1) and triplet (T_1) excited states together with the wave functions were calculated by the TD-DFT CAM-B3LYP/TZVD/MWB52 method, including the effect of the DCM solvent. The energy of S_1 and T_1 and their respective distance (R_L) between the acceptor and the donor for each state of both complexes are presented in **Table 2**. A comparison of R_L of the complexes indicated that the energy of the donor (S_1 and T_1) states is slightly farther away in the case of **Eu-2**. This could be due to the greater structural extension of the β-diketonate coordinated to Eu(III) in **Eu-2**. An analysis of the MOs further revealed that the electronic transitions that comprise S_1 and T_1 states (**Table 2**) are derived from the MOs centred on both β-diketonate and Ph-TerPy ligands (**Fig. 6 & 7**). Since the composition of T_1 for the

complexes is similar, only a small energy difference between the states is expected (22,838.1 *vs.* 22,463.4 cm^{-1}).

Table 2: Energy of the lowest singlet and triplet excited states, electronic transitions for the respective excited states, and corresponding distance from energy donor to acceptor centre (R_L) of **Eu-1** and **Eu-2** determined by the CAM-B3LYP/TZVP/MWB52 method.

Compound	State	Energy/cm^{-1}	R_L/Å	Major Contribution	Total
Eu-1	S_1	33,407.8	4.53	HOMO-13→LUMO+1 (16.97% HOMO-12→LUMO+1 (10.51%) HOMO-14→LUMO+1 (10.37%) HOMO-13→LUMO+4 (7.45%) HOMO-11→LUMO+1 (6.56%)	51.87%
	T_1	22,838.1	4.45	HOMO-1→LUMO+2 (48.63%) HOMO-1→LUMO+4 (23.19%) HOMO-1→LUMO+1 (12.84%)	84.66%
Eu-2	S_1	32,785.0	4.74	HOMO-2→LUMO+2 (16.15%) HOMO-1→LUMO+1 (11.05%) HOMO→LUMO+1 (10.39%) HOMO→LUMO+3 (10.11%) HOMO-1→LUMO (8.58%)	56.28%
	T_1	22,463.4	4.84	HOMO-3→LUMO+3 (12.18%) HOMO-3→LUMO+2 (11.19%) HOMO-2→LUMO+3 (9.83%) HOMO→LUMO+3 (7.56%) HOMO-2→LUMO+2 (7.05%) HOMO→LUMO+2 (5.92%)	53.72%

The ET rate involving two excited states is calculated with the help of the distance R_L and of the energy difference of the excited states (term Δ presents in Eq. S4). Furthermore, the ET rates due to the direct Coulombic interaction (CI) mechanism is a function of the forced electric dipole (FED) intensity parameters (Ω_λ^{FED}), which were calculated (**Table S3, ESI**) by the *QDC*

model[28] developed by one of us and implemented in LUMPAC[14] software package. The theoretical Ω_2 and Ω_4 values (**Table 1)** obtained by the *QDC* model agree well with the experimental values, implying that the theoretical methods applied in the calculations are an excellent choice. A comparison between Ω_λ^{FED} and Ω_λ^{DC} (**Table S3, ESI**) substantiates that the emission of the complexes is governed by the DC mechanism and J-O parameters are greatly dependent on the polarizabilities of the atoms directly coordinated to the Eu(III) ion.

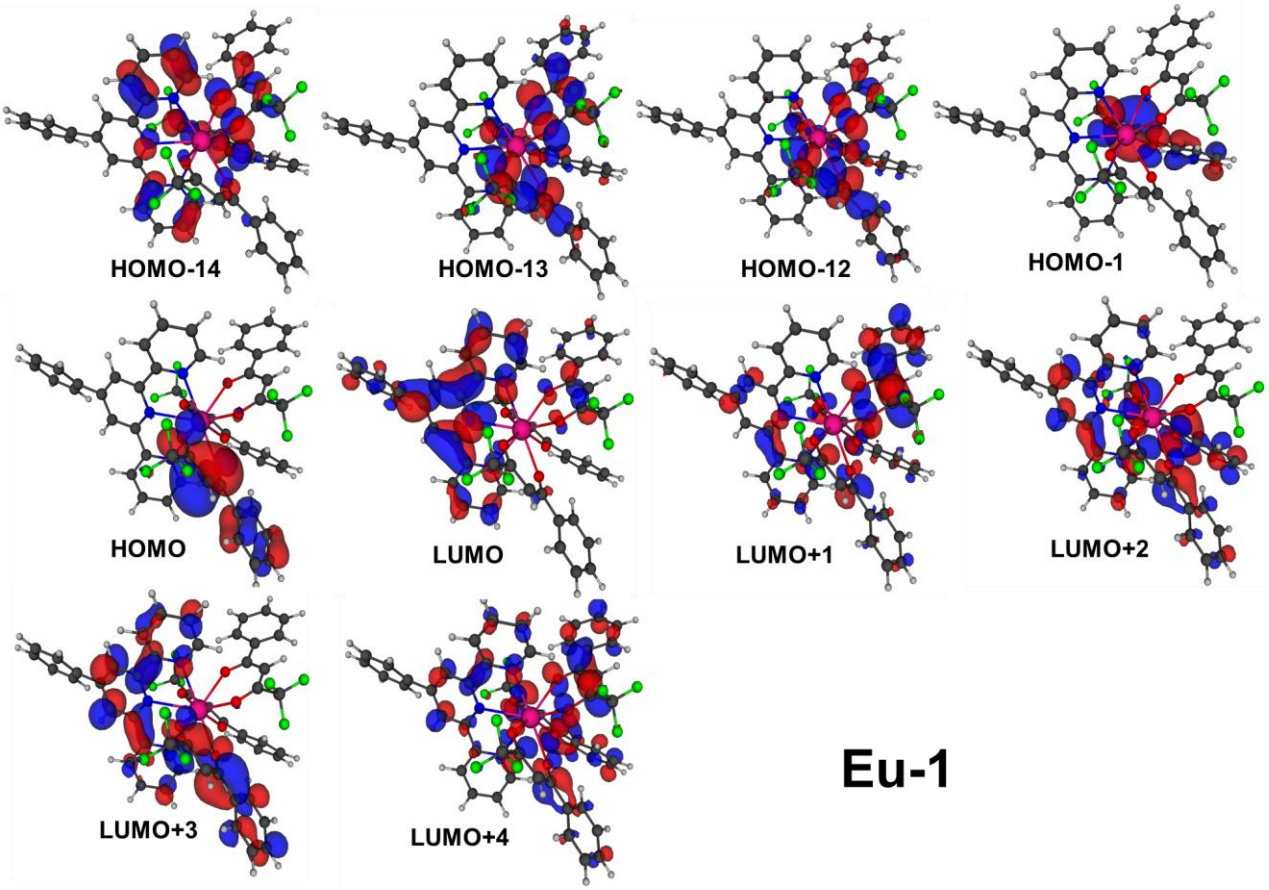

Figure 6: MOs predicted at the TD-DFT CAM-B3LYP/TZVD/MWB52 level of theory, considering the effect of the DCM solvent for **Eu-1**.

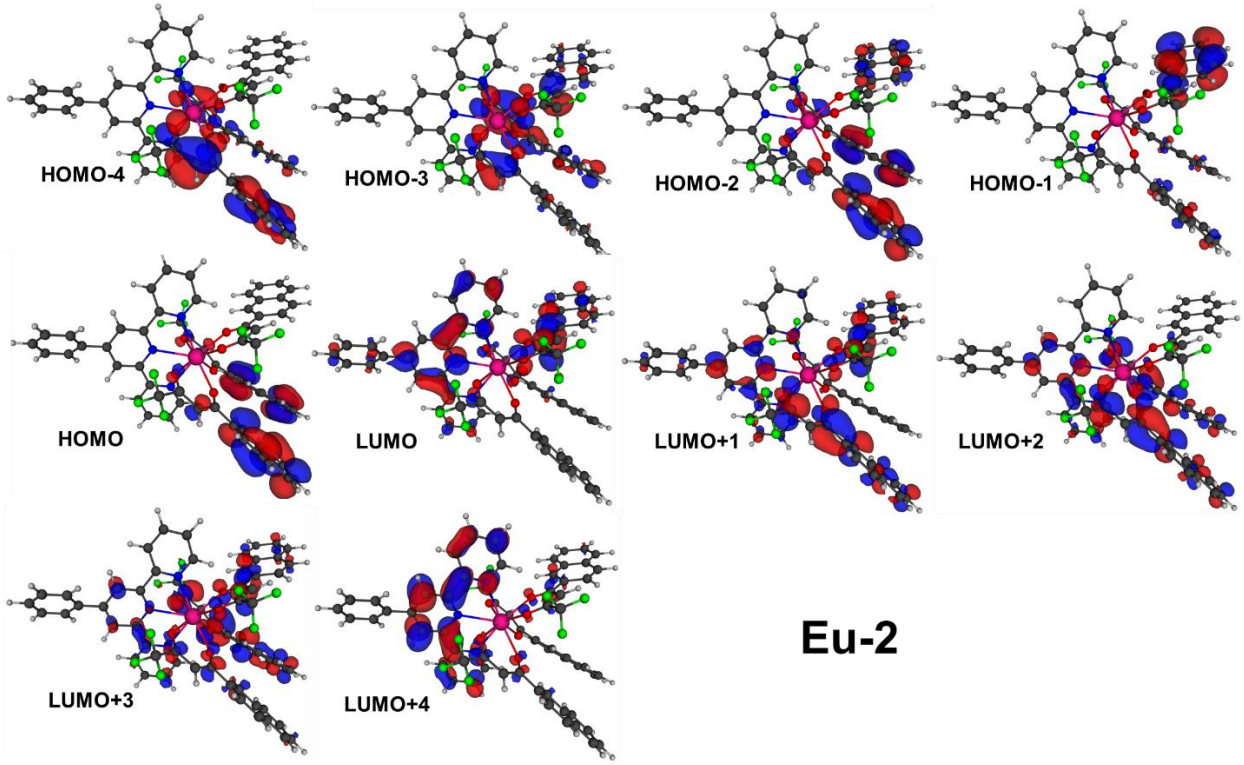

Figure 7: MOs predicted at the TD-DFT CAM-B3LYP/TZVD/MWB52 level of theory, considering the effect of the DCM solvent for **Eu-2**.

The ET rates calculated using Malta's model [29] for the **Eu-1** and **Eu-2** complexes involving the S_1 and T_1 states of the ligands and different excited levels of the Eu(III) ion ($^5D_0$, $^5D_1$, $^5D_2$, $^5D_3$, $^5D_4$, $^5L_6$, $^5L_7$, $^5G_2$, $^5G_3$, $^5G_5$, and $^5G_6$) are listed in **Table S4**. A total of 180 ET rates are calculated (90 for each complex, out of which 30 for CI, 30 for Ex. mechanism and 30 for backward ET, please see **Table S4**). A comparison between the ET pathways that involve S_1 and T_1 state for both the complexes reveals a rate of an order of 10^7 s^{-1} for $^7F_0 \rightarrow {}^5D_1$ and $^7F_1 \rightarrow {}^5D_0$ excitations which is allowed by the Ex. mechanism, while the largest rate of 10^5 s^{-1} ($^7F_1 \rightarrow {}^5G_2$ and $^7F_1 \rightarrow {}^5G_3$) is observed for the ET channel, which involves S_1. This observation implies that the $T_1 \rightarrow {}^5D_0$ and $T_1 \rightarrow {}^5D_1$ channels are the most important in sensitizing the PL of the present complexes. Moreover, backward ET (W_{BET}) rates involving S_1 and $^5D_4$ (27,586 cm^{-1}) excited state is nearly equal to zero; however, large W_{BET} values were observed for the T_1 and some excited states due to good resonance condition.

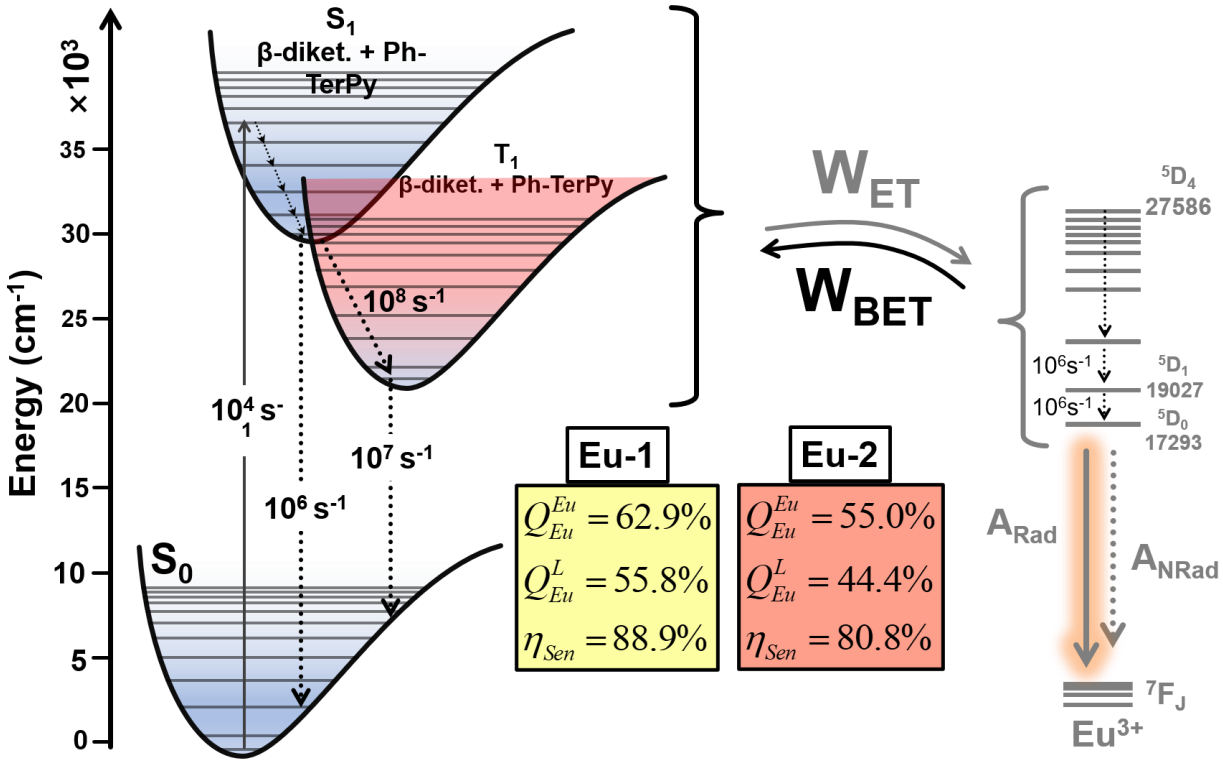

Figure 8: Jablonski diagram showing the states included in the process of ET of the complexes.

Fig. 8 shows an energy level diagram that illustrates the ligand-to-Eu(III) ET processes. To reproduce the experimental η_{Sen} for the present complexes, the ligand decay rates [30] $S_1 \rightarrow S_0$ (10^6 s^{-1}), $S_1 \rightarrow T_1$ (10^8 s^{-1}), and $T_1 \rightarrow S_0$ (10^7 s^{-1}) were adjusted and the method is detailed in our very recent works.[1a, 1c] By considering the above mentioned ligand rates the theoretical η_{Sen} equal to 88.9% and 80.8%, respectively, were obtained and these values agree very well with the experimental data (**Table 1**) suggesting the efficacy and suitability of the applied theoretical method to reproduce the experimental photophysical results. It is important to emphasize that the ET rates for both complexes have the same order of magnitude; however, it is not responsible for the difference of η_{Sen} of the complexes. A plausible explanation of the lower quantum yield of **Eu-2** compared to **Eu-1** could be attributed to the large A_{NRad} = 986.79 s^{-1} of **Eu-2,** which is further due to the greater number of C-H oscillators.

EL Properties and Performances of Eu-1 and Eu-2

Before realizing good EL properties and using newly synthesized materials (here **Eu-1** & **Eu-2**) in an efficient device fabrication process, it is critically important to establish the thermal stability of the emitting materials since poor thermal stability hampers the performance and life-time of the optoelectronic devices at the peak of its operation due to the Joule heating effect when current flows through the organic layers.[1a, 1b] Thermal stability of the complexes was evaluated in the temperature range between 50 and 700 °C. The thermograms of the complexes (**Fig. 9**, **Fig. S3** & **Fig. S5**, **ESI**) demonstrated that **Eu-1** and **Eu-2** possess good thermal stability with T_d (with 5% weight loss) of 313.36 °C for **Eu-1** and 287.04 °C for **Eu-2**, respectively. The high thermal stability of the complexes implies that they can be readily employed to fabricate OLEDs by the VTE method.

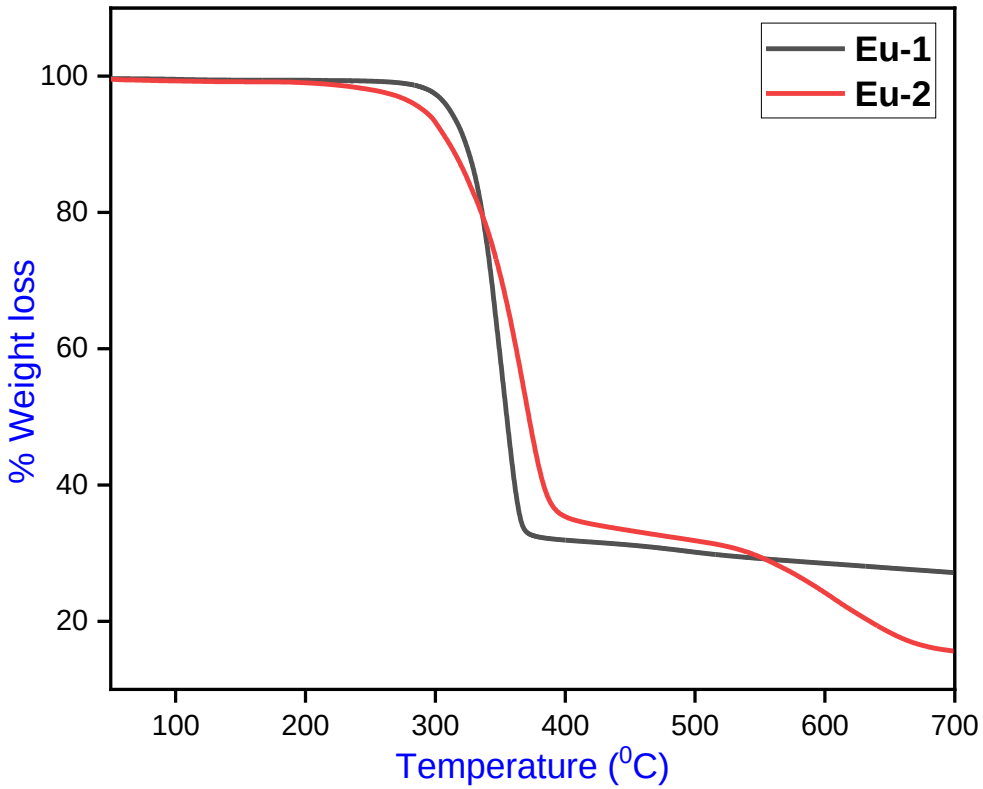

Figure 9: Thermograms of **Eu-1** and **Eu-2** under N_2 atmosphere.

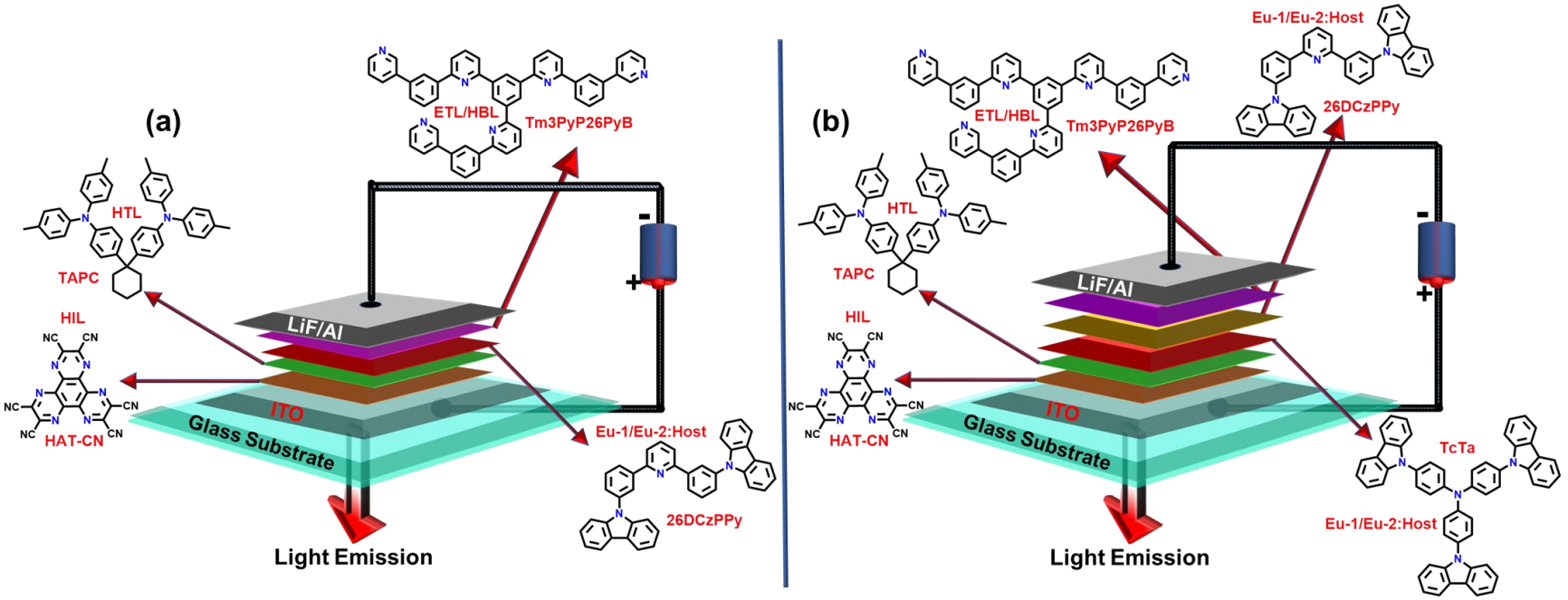

Figure 10: General device configuration (a) single-EML and (b) double-EML OLEDs (where = HIL: Hole Injection Layer; HTL: Hole Transport Layer; ETL: Electron Transport Layer; HBL: Hole Blocking Layer; HAT-CN: 1,4,5,8,9,11-hexaazatriphenylene hexacarbonitrile; TAPC: Di-[4-(N,N-ditolyl-amino)-phenyl]cyclohexane; Tm3PyP26PyB: 1,3,5-Tris(6-(3-(pyridin-3-yl)phenyl)pyridin-2-yl)benzene; **Host**: (26DCzPPy: 2,6-bis(3-(9H-carbazol-9-yl)phenyl)pyridine; TcTa: 4,4',4''-Tris(carbazole-9-yl)triphenylamine). Specific details of the different composition are included the ESI.

To produce an efficient ET process in the device it is important that the host emission spectrum should overlap with the absorption spectrum of the guest emitter.[31] As can be seen from **Fig. S16, ESI** that there is good spectral overlap between the absorption spectra of complexes and host emissions (26DCzPPy and TcTa) suggesting the possibility of achieving high-performance device. Finally, to study the potential of the synthesized complexes as an EML, 10 single-EML and 10 double-EML OLEDs were fabricated by VTE method as shown in **Fig. 10** by varying the doping concentration of the complexes. It is important to emphasize that as the doping concentration increases, there is a gradual increase in the evaporation temperature [165–176 °C for **Eu-1** and 152–159 °C for **Eu-2**]; however, it remained lower for both the T_m and T_d. The EL spectra and performances such as B, η_c, η_p, and EQE were determined and are summarized in **Table 3**. The EL spectra of all devices (**Fig. 11** and **Figs. S17 & S18, ESI**) displayed typical well-resolved Eu(III) emission transition originating from the $^5D_0 \rightarrow {}^7F_J$ (J = 0 – 4). The EL spectra mimic the PL spectra (**Figs. S19 & S20, ESI**) in the region between 530 and 750 nm and suggest that the recombination of electrons and holes were successfully confined to the Eu(III) complex molecules.[1c]

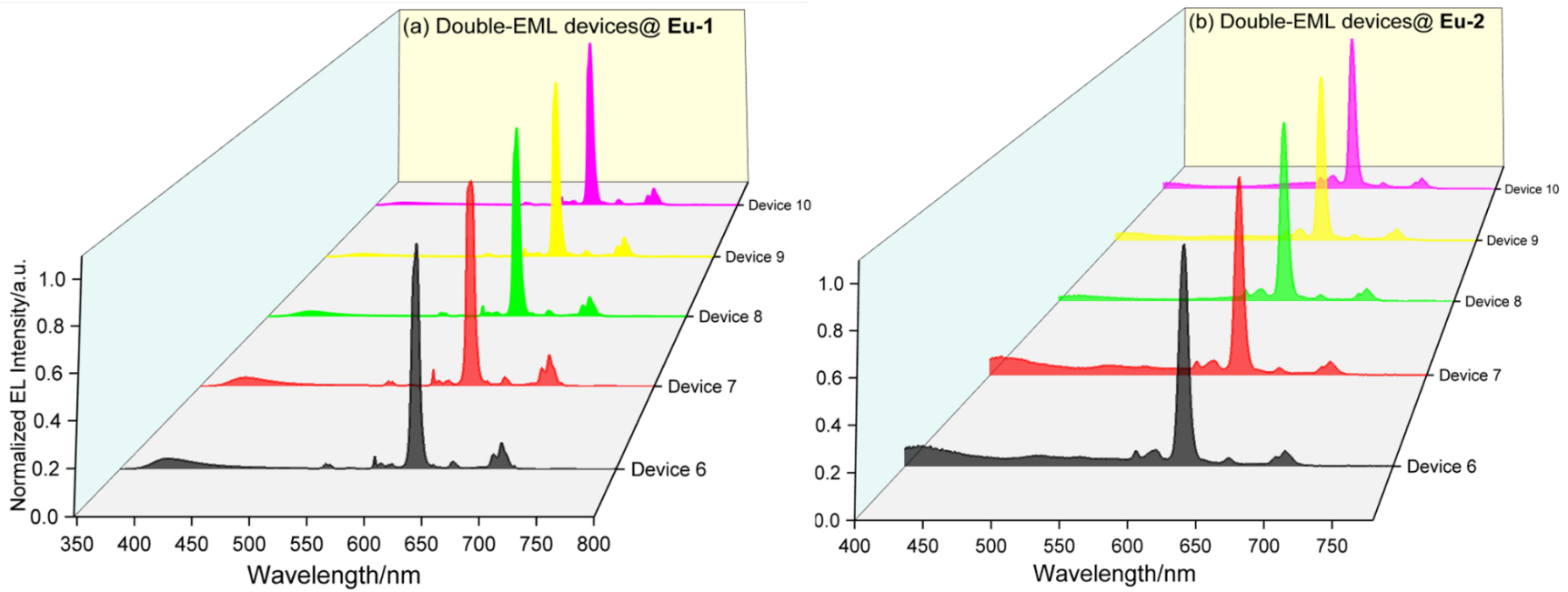

Figure 11: Normalized EL spectra of double-EML devices of **Eu-1** and **Eu-2** at different doping concentrations operating at J = 10 mA/cm^2.

Besides this, the EL spectra displayed host emission; however, as the doping concentration increases, the intensity of the host emission decreases (**Figs. S21** – **S24, ESI**). This could be attributed to the participation of more Eu(III) complex molecules in the EL process and points towards improved Foster ET from the host to the europium complexes. [1c] The **Eu-1** based single-EML devices displayed red EL at all doping concentrations (Table 3 & **Fig. S25**, **ESI**); however, the colour of **Eu-2** based single-EML devices are magenta to red (Table 3 & **Fig. S26**, **ESI**) due to the presence of host (26DCzPPy) emission. To further improve the EL performances of double-EML devices comprising two different host materials, devices were fabricated for both complexes keeping the same doping concentration i.e., 1 – 5 wt%. EL spectra of the devices displayed combined emissions of both hosts (**Figs S27** & **S28**, **ESI**) with a similar trend as observed for single-EML devices i.e., host emission decreases gradually with increasing doping concentration. It is important to note that the double-EML devices displayed relatively weaker host emission compared to the single-EML devices (**Figs. S29 & S30, ESI**), which could be attributed to the wider recombination zone that certainly will help to facilitate the ET from host to emitter since more europium(III) molecules will participate in the EL processes.[12a] At the optimum doping concentration i.e., **device 9** of **Eu-1** and **device 8** of **Eu-2** displayed red emission (**Fig. S31, ESI**).

Table 3: Key EL performances of single- and double-EML devices based on **Eu-1** and **Eu-2**.

Device	$V_{turn\text{-}on}$ (V)	B[a] (cd/m^2)	η_c[b] (cd/A)	η_p[c] (lm/W)	EQE (%)[d]	$CIE_{x,y}$[e]
Eu-1						
1 [6]	3.3 [3.4]	1845 [1564]	3.52 [4.83]	3.15 [4.10]	2.5 [3.4]	0.602, 0.305 [0.644, 0.315]
2 [7]	3.4 [3.6]	1516 [1222]	4.63 [5.04]	3.83 [3.68]	3.3 [3.6]	0.643, 0.315 [0.652, 0.319]
3 [8]	3.5 [4.0]	1321 [1023]	4.88 [5.07]	4.22 [4.24]	3.5 [3.6]	0.649, 0.320 [0.657, 0.320]
4 [9]	3.3 [3.6]	958 [1179]	5.33 [5.64]	4.71 [4.78]	3.8 [4.0]	0.658, 0.322 [0.663, 0.663]
5 [10]	3.6 [4.0]	886 [624]	4.27 [4.73]	3.35 [3.45]	3.0 [2.4]	0.654, 0.320 [0.658, 0.320]
Eu-2						
1 [6]	2.9 [3.1]	555 [778]	4.14 [8.48]	4.49 [8.60]	3.12 [5.78]	0.46, 0.30 [0.47, 0.30]
2 [7]	2.9 [3.1]	490 [805]	5.34 [9.33]	5.78 [9.45]	4.33 [7.08]	0.49, 0.29 [0.47, 0.31]
3 [8]	2.9 [3.1]	574 [838]	7.45 [10.19]	8.08 [10.33]	5.40 [7.32]	0.52, 0.30 [0.59, 0.32]
4 [9]	3.0 [3.2]	523 [716]	5.60 [8.91]	5.86 [8.75]	4.74 [7.75]	0.49, 0.31 [0.54, 0.32]
5 [10]	3.1 [3.3]	539 [818]	5.15 [8.30]	5.21 [7.90]	3.69 [5.26]	0.53, 0.33 [0.55, 0.35]

Values in the square bracket are for double-EML devices

[a]The data for maximum brightness (B); [b]maximum current efficiency (η_c); [c]maximum power efficiency (η_p); [d]maximum external quantum efficiency (EQE); [e]$CIE_{x,y}$ at 10 mA/cm^2

The EL efficiency and current density curves, together with the voltage (V)-brightness (B) and current density (J) curves as an inset for the single- and double-EML devices are shown in **Fig. 12 and Figs. S32 & S33, ESI**. Key EL performances of the devices based on **Eu-1** and **Eu-2** such as B, η_c, η_p, EQE and CIE colour coordinates are summarized in **Table 3**. As can be seen from **Table 3**, η_c increases as the doping concentration increases and then decreases and this possibly is due to the imbalance between the hole-electron pair within the EML. This will break the balance of holes and electrons within EML and thus will lead to the decrease in η_c which in turn is related to EQE.[1c] At the optimum doping concentration, the single-EML devices i.e., Device 4 and Device 3 of **Eu-1** and **Eu-2**, respectively, displayed impressive red ($CIE_{x,y}$ = 0.658, 0.322) and magenta ($CIE_{x,y}$ = 0.52, 0.30) EL with B = 958 cd/m^2, η_c = 5.33 cd/A, η_p = 4.71 lm/W and EQE = 3.8% at very low $V_{turn\text{-}on}$ = 3.3 V for **Eu-1** based device and B = 838 cd/m^2, η_c = 7.45 cd/A, ηp = 8.08 lm/W and EQE = 5.40% at very low $V_{turn\text{-}on}$ = 2.9 V for **Eu-2** based device at a J = 10 mA/cm^2. It is noteworthy that devices displayed very low turn-on voltage, which implies barrier-free carrier injection, balanced carrier transport and recombination.[1c] In order to further improve the EL performances of the devices one more EML (double EMLs) with TcTa host having hole transporting ability (3.1×10^{-4} cm^2 V^{-1} s^{-1})[32] is introduced. The introduction of the second EML has a marginal improvement on the EL performances of **Eu-1** based devices. At the optimum doping concentration i.e., **Device 9** exhibited red EL with B = 1179 cd/m^2, η_c = 5.64 cd/A, η_p = 4.78 lm/W, EQE = 4.0% and very low $V_{turn\text{-}on}$ = 3.6 V at J = 10 mA/cm^2, which are higher than most of the highly efficient OEuCs based OLEDs (**Table 4 and Fig. 13**). Interestingly and to our surprise, the EL performances of the double-EML device at the optimum concentration i.e., **Device 8** displayed overall remarkable EL performances with the B = 838 cd/m^2, η_c = 10.19 cd/A, η_p = 10.33 lm/W, EQE = 7.32% and very low $V_{turn\text{-}on}$ = 3.1 V at J = 10 mA/cm^2, which are almost two-fold higher than those of **Eu-1** based device. The higher EL performance of **Eu-2** based device could possibly be due to the presence of three terminal electron-rich napthyl rings of β-diketone leading to more balanced carrier transport than **Eu-1** having three phenyl ring terminal

rings. This is further supported by the very recent report on the EL performance of ytterbium complex of 2-(tosylamino)-benzylidene-N-(2-halobenzoyl)-hydrazones where the substitution of a benzoyl ring with naphthyl resulted in a significant increase of the electron mobility (6.9×10^{-7} vs. 1.7×10^{-6} cm^2 V^{-1} s^{-1}).[33] It is important to note that the device performances of the present **Eu-2** based OLEDs are among the best reported in the literature [34] (**Table 4** and **Fig. 13**) so far with EQE exceeding 7.0% at J = 10 mA/cm^2.

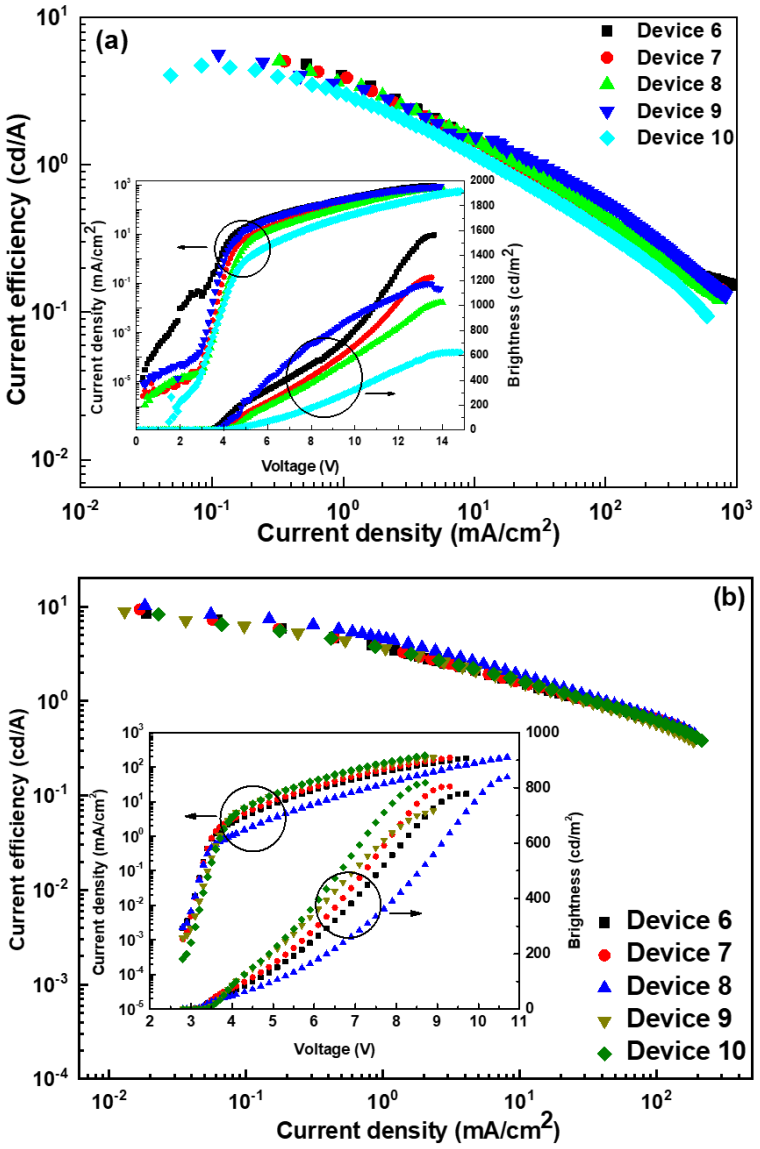

Figure 12: EL efficiency-current density characteristics. Inset: Current density-brightness-voltage characteristics of devices **6**, **7**, **8, 9** and **10** of (a) **Eu-1** and (b) **Eu-2** based double-EML devices

.

Table 4. Comparative EL performances of reported Eu-CCs (their chemical structures are shown in **Chart 2)**.

Emitting Layer	$V_{turn-on}$ V	B^a cd/m^2	$\eta_c{}^b$ cd/A	$\eta_p{}^d$ lm/W	EQE %	$CIE_{x,y}{}^e$	Reference
Eu-1(4 wt%):TcTa (10 nm)/**Eu-1** (4 wt%): 26DCzPPy (10 nm)	3.6	1179	5.64	4.78	4.0	0.663, 0.663	This work
Eu-2 (3 wt%):TcTa (10 nm)/ **Eu-2** (3 wt%):26DCzPPy (10 nm)	3.1	838	10.19	10.33	7.32	0.59, 0.32	This work
Eu-3 (3 wt%) : 26DCzPPy (10 nm)	3.5	2108	8.45	6.98	6.0	0.628, 0.308	[7]
Eu-4 (5 wt%) : PBD (90 nm)	–	–	10.0	–	5.30	–	[35]
Eu-5 (90 nm) : CBP : PBD	–	–	5.1	1.0	3.70	0.66,0.33	[36]
Eu-6 (40 nm)	5.0	–	5.88	3.69	3.71	–	[37]
Eu-7 (80 nm) : PBD	7.4	1333	2.61	–	1.80	0.544,0.382	[38]
Eu-8 : CBP (40 nm, 10%)	7.6	1276	–	–	3.54	–	[39]
Eu-9 (40 nm)	5.7	–	5.07	3.62	3.20	–	[37]
Eu-10 : CBP (40 nm, 10%)	7.2	1163		–	3.20	–	[39]
Eu-11: CBP (40 nm, 10%)	6.0	945	–	–	2.96	–	[39]
Eu-12 : CBP (30 nm, 10%)	7	632	4.58	2.89	2.89	–	[40]
Eu-13 (90 nm) : CBP : PBD	–	–	3.2	0.6	2.40	0.65,0.32	[36]
Eu-14 (3 wt%) : 26DCzPPy (10 nm)	4.0	1237	3.09	2.33	2.2	0.639, 0.318	[7]
Eu-15 (8%) : TCTA (10 nm)/**Eu-15** (8%) : 26DCzPPy (10 nm)	3.4	428	3.31	3.06	2.14	0.619, 0.323	[41]
Eu-16 (10 wt%) : TCTA : Bphen	2.9	–	3.85	2.26	2.12	–	[35]
Eu-17 (40 nm)	8.4	–	3.25	1.23	2.08	–	[37]
Eu-18 (8 wt%**)** : CBP (30 nm, 8%)	19.8	1365	3.31	–	1.80	–	[42]
Eu-19 (8%) : TCTA (10 nm)/**Eu-19** (8%) : 26DCzPPy (10 nm)	3.4	896	2.26	1.92	1.6	0.640, 0.311	[1c]
Eu-20 (90 nm) : CBP : PBD	12	278	–	–	1.45	–	[43]

Where BPhen = 4,7-diphenyl-1,10-phenanthroline; PBD = 2-(tert-butylphenyl)-5-biphenylyl-1,3,4-oxadiazole; CBP = 4,4'-N,N'-dicarbazole-biphenyl.

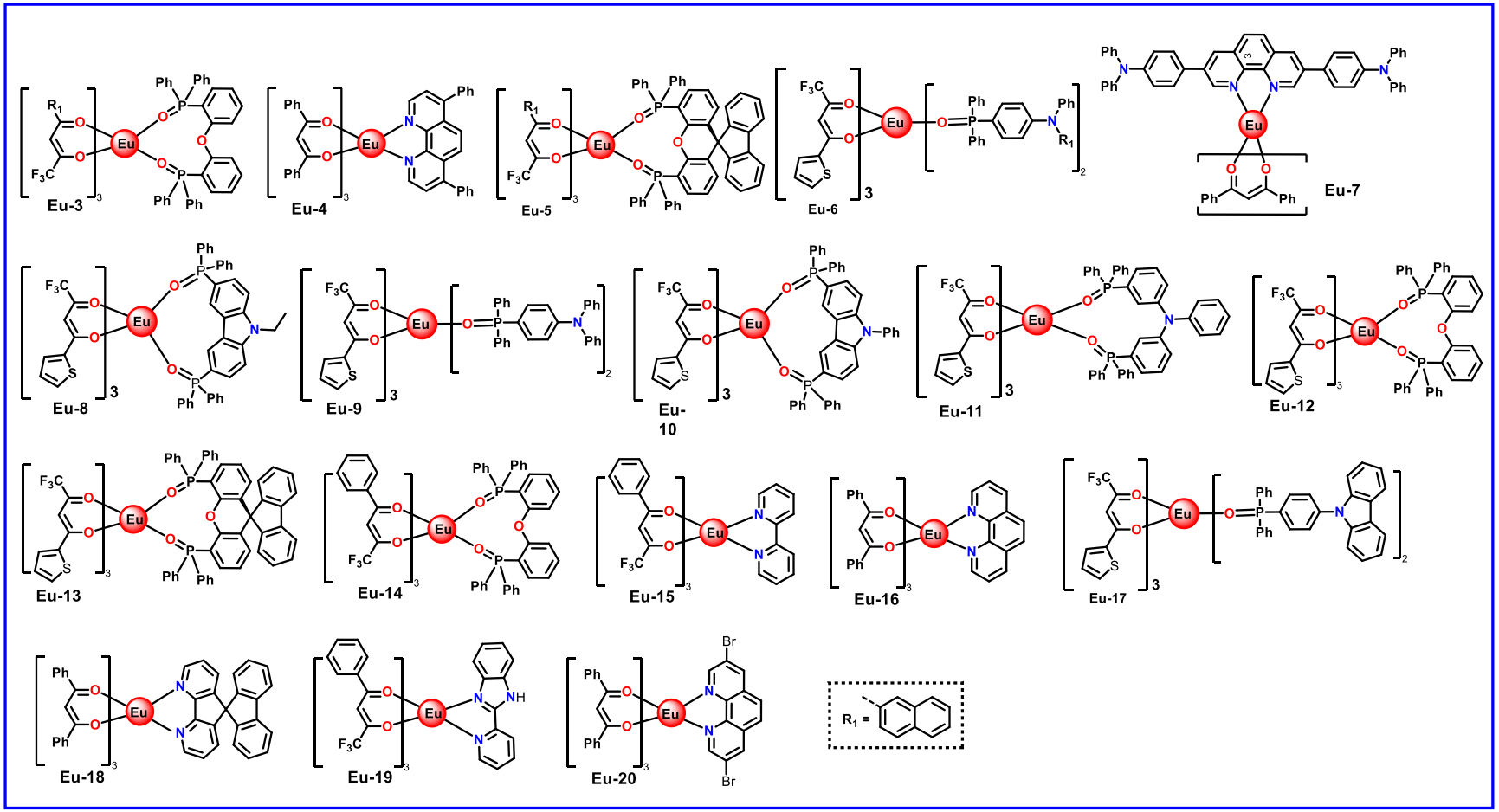

Figure 13: Chemical structures of some reported efficient ternary OEuCs.

Conclusion

In summary, two nona coordinate red-emitting ternary Eu(III) complexes were successfully synthesized. The geometry of the complexes was determined by the DFT method. An analysis demonstrated that the coordination geometry around Eu(III) centre in **Eu-2** is a distorted spherical capped square antiprism (C_{4v}) which is more asymmetrical than **Eu-1** with a distorted spherical tricapped trigonal prism (D_{3h}). Both the complexes displayed typical Eu(III) pure red emission with short τ_{obs} = 600.15 ± 2.14 μs and 449 ± 1.01 μs and large Q_{Eu}^{L} = 54.90 % and 44.95 % for **Eu-1** and **Eu-2,** respectively. The shorter τ_{obs} for **Eu-2** compared to **Eu-1** could be associated with the highly asymmetric coordination geometry and was further supported by the large values of R_{21} = 18.81 and Ω_2 = 33.32 × 10^{-20} cm^2. ET mechanism indicated that $T_1 \rightarrow {}^5D_0$ and $T_1 \rightarrow {}^5D_1$ channels are the most important for the sensitized PL in these complexes with the same order of W_{ET} (10^7 s^{-1}). Despite identical ET rates, Q_{Eu}^{L} of **Eu-2** is 10.0% lower than **Eu-1** and could be associated with the large A_{NRad} = 986.79 s^{-1} of **Eu-2**. Finally, we have shown the potential application of the complexes as an EML to fabricate bright and red OLEDs that could be employed as a component to fabricate white-OLEDs *via* the RGB method for portable full color flat displays. At the optimum doping concentration, the double-EML device of **Eu-2** exhibited almost two-fold higher EL performances than those of **Eu-1** based double-EML device despite 10% lower PLQY, demonstrating the higher significance of charge mobility over PLQY. The overall EL performances of the **Eu-2** based device i.e., B = 838 cd/m^2, η_c = 10.19 cd/A, η_p = 10.33 lm/W, EQE = 7.32%, and $V_{turn\text{-}on}$ = 3.1 V at J = 10 mA/cm^2 are the highest values reached by an OEuC (**Table 4** and **Fig. 13**). Further investigation to improve the EL performance of OEuCs by introducing different charge carrier group(s) is underway in our laboratory.

Synthesis

4'-Phenyl-2,2':6',2''-terpyridine (Ph-TerPyr) and OEuCs

The tridentate Ph-TerPyr ligand was synthesized by the reported method.[44] Briefly, to a stirred solution of benzaldehyde (1.8422 g; 17.36 mmol) and 2-acetylpyridine (4.2084 g, 34.74 mmol) in 50 mL of ethanol (EtOH), potassium hydroxide (KOH; 1.95 g; 38.50 mmol) and 25% ammonia solution (15 mL) were added. The reaction mixture was stirred for 24 h at room temperature. The precipitate was isolated by vacuum filtration and washed with a copious amount of distilled water, followed by EtOH (50 mL × 2). Analytically pure compound was obtained by recrystallization from dichloromethane (CH_2Cl_2): EtOH (1:1) as colourless crystals (60% yield).

[Eu(btfa)$_3$(Ph-TerPyr)] (Eu-1)

Eu-1 was synthesized by reacting equimolar quantities of [Eu(btfa)$_3$(H_2O)$_2$][7] (0.300 g; 0.360 mmol) and Ph-TerPyr (0.111 g; 0.360 mmol) in methanol (MeOH; 20 mL). The reaction mixture was stirred overnight at room temperature and left for slow solvent evaporation. The solid formed was washed with cold EtOH (5 × 2 mL) and toluene (5 × 2 mL). Yield 80%. Microanalysis calculated for $C_{51}H_{33}EuF_9N_3O_6$, C, 55.35; H, 3.01; N, 3.80; observed C, 55.40; H, 3.08; N, 3.76. FTIR (solid; cm^{-1}): v(ar C-H st) 3051 cm^{-1}; v(C=O st) 1,612 cm^{-1}; v(C=N st) 1,576 cm^{-1}; v(C=C st) 1,507 cm^{-1}; v(C-F st, CF_3) 1371, 1309 cm^{-1}; out-of plane asymmetric v(C-F st) 1,178 cm^{-1}; in-plane v(C-H bend) 1,124 cm^{-1} (**Fig. S1a, ESI**); ESI-MS$^+$: m/z: 1200.9 for [**Eu-1**+Na+(CH_3CN)+(CH_3OH)-H]$^+$ (**Fig. S2, ESI**); Melting temperature (T_m) = 236.30 °C; Decomposition temperature (T_d) with 5% weight loss = 313.36 °C (**Fig. S3, ESI**).

[Eu(NTA)$_3$(Ph-TerPyr)] (Eu-2)

Eu-2 was obtained by a similar method. [Eu(NTA)$_3$(H_2O)$_2$][7] (0.300 g; 0.305 mmol) and Ph-TerPyr (0.943 g; 0.305 mmol) in methanol (MeOH; 20 mL) Yield 75%. Microanalysis calculated for $C_{63}H_{39}EuF_9N_3O_6$, C, 60.20; H, 3.13; N, 3.34; observed C, 60.19; H, 3.10; N, 3.31. FTIR (solid; cm^{-1}): v(ar C-H st) 3068 cm^{-1}; v(C=O st) 1,613 cm^{-1}; v(C=N st) 1,570 cm^{-1}; v(C=C st) 1,507 cm^{-1}; v(C-

F st, CF_3) 1388, 1292 cm^{-1}; out-of plane asymmetric v(C-F st) 1,181 cm^{-1}; in-plane v(C-H bend) 1,122 cm^{-1} (**Fig. S1b, ESI**); ESI-MS^+: m/z :1279.8 for [**Eu-2**+Na]$^+$ (**Fig. S4, ESI**); T_m = not observed; Decomposition temperature (T_d) with 5% weight loss = 287.04 °C (**Fig. S5, ESI**).

Spectroscopic measurements, photophysical parameters and computational chemistry

Spectroscopic measurements of **Eu-1** and **Eu-2** including optical absorption, excitation, emission spectra, decay profiles and absolute PLQY values were obtained at room temperature; details of the measurements have been reported previously.[7] Optical absorption spectra were obtained using Varian Cary 5000 UV-Visible-NIR spectrophotometer while excitation, emission spectra and decay profiles were recorded on an Edinburgh FS5 fluorimeter. The absolute PLQY were determined using a calibrated integrating sphere on a C-9920-02 from the Hamamatsu Photonic instrument. Photophysical parameters such as the J-O parameters (Ω_2 and Ω_4), A_{Rad}, A_{NRad} decay rates, radiative lifetime (τ_{rad}), Q_{Eu}^{Eu} and η_{sen} were calculated by applying the following set of equations and details are reported elsewhere. [3a]

$$\Omega_{\lambda}^{\exp} = \frac{3\hbar A_{Rad}\left[{}^5D_0 \rightarrow {}^7F_J\right]}{32e^2\pi^3\chi\nu\left[{}^5D_0 \rightarrow {}^7F_J\right]^3\left|\left\langle {}^5D_0\left\|U^{(\lambda)}\right\|{}^7F_J\right\rangle\right|^2} \quad \text{Eq. 1}$$

$$A_{Rad} = \sum_{J=0}^{4} A_{Rad}\left[{}^5D_0 \rightarrow {}^7F_J\right] \quad \text{Eq. 2}$$

$$A_{Rad}\left[{}^5D_0 \rightarrow {}^7F_J\right] = \frac{\nu\left[{}^5D_0 \rightarrow {}^7F_1\right]}{\nu\left[{}^5D_0 \rightarrow {}^7F_J\right]} \times \frac{A\left[{}^5D_0 \rightarrow {}^7F_J\right]}{A\left[{}^5D_0 \rightarrow {}^7F_1\right]} A_{Rad}\left[{}^5D_0 \rightarrow {}^7F_1\right] \quad \text{Eq. 3}$$

$$A_{tot} = \frac{1}{\tau_{obs}} = A_{Rad} + A_{NRad} \quad \text{Eq. 4}$$

$$\tau_R = 1 \Big/ A_{Rad} \quad \text{Eq. 1}$$

$$Q_{Eu}^{Eu} = \frac{\tau_{obs}}{\tau_{Rad}} = \frac{A_{Rad}}{A_{Rad} + A_{NRad}} \quad \text{Eq. 2}$$

$$\eta_{sen} = \frac{Q_{Eu}^{L}}{Q_{Eu}^{Eu}}$$ Eq. 7

The theoretical methodology which includes the determination of the ground-state geometry, theoretical absorption spectrum, ET rates, radiative emission rate (A_{Rad}) and theoretical PLQY is detailed in the electronic supporting information.

Fabrication of EL devices and assessments of their EL performance

Indium tin oxide (ITO) coated glass with sheet resistance of 10 Ω/sq was used as the anode substrate. Prior to film deposition, patterned ITO substrates were cleaned with detergent, rinsed in de-ionized water, and finally dried in an oven. All organic layers were deposited at the rate of 0.1 nm/s under high vacuum (≤ 3.0×10^{-5} Pa). The doped EMLs were prepared by co-evaporating dopant and host material from two sources, and the doping concentration was modulated by controlling the evaporation rate of the dopant. Lithium fluoride (LiF) and aluminium (Al) were deposited in another vacuum chamber (≤ 8.0×10^{-5} Pa) at the rates of 0.01 and 1.0 nm/s, respectively, without being exposed to the atmosphere. The thicknesses of these deposited layers and the evaporation rate of individual materials were monitored in vacuum with quartz crystal monitors. A shadow mask was used to define the cathode and make eight emitting dots with an active area of 9 mm^2 on each substrate. Current density (J)-brightness (B)-voltage (V) characteristics were measured by using a programmable brightness light distribution characteristics measurement system C9920-11 from the Hamamatsu Photonic instrument. PL and EL spectra were measured with a calibrated Hitachi F−7000 fluorescence spectrophotometer and an Ocean Optics spectrophotometer.

Acknowledgements

MSK acknowledges His Majesty's Trust Fund for Strategic Research (Grant No. SR/SQU/SCI/CHEM/21/01) and The Ministry of Higher Education, Research and Innovation (MoHERI), Oman (Grant: RC/RG-SCI/CHEM/23/01) for funding. RI thanks HM's Trust Fund for a

postdoctoral fellowship. JDLD appreciates the financial support from the Brazilian funding agencies CAPES, CNPq (421733/2018-7), FACEPE (APQ-0675-1.06/14) and FAPITEC-SE (FAPITEC/SE/FUNTEC Nº 06/2021), and thanks Gabriel Silva Santos for calculating the ligand decay rates and the emission quantum yield of the compounds. LZ is grateful for the financial aid from the National Natural Science Foundation of China (62174160). WYW thanks the Hong Kong Research Grants Council (PolyU 15305320), Guangdong-Hong Kong-Macao Joint Laboratory of Optoelectronic and Magnetic Functional Materials (2019B121205002), the CAS-Croucher Funding Scheme for Joint Laboratories (ZH4A), Hong Kong Polytechnic University, Research Institute for Smart Energy (CDAQ) and the Endowed Professorship in Energy from Miss Clarea Au (847S) for the financial support. PRR is grateful to the Engineering and Physical Sciences Research Council (EPSRC) for funding (Grant EP/K004956/1).

Conflict of Interest

The authors declare no conflict of interest.

Data Availability Statement

The data that support the findings of this study are available in the supplementary material of this article**.**

References

[1] (a) R. Ilmi, J. Yin, J. D. L. Dutra, N. K. Al Rasbi, W. F. Oliveira, L. Zhou, W. Y. Wong, P. R. Raithby, M. S. Khan, *Dalton Trans* **2022**, *51*, 14228-14242; (b) R. Ilmi, D. Zhang, L. Tensi, H. Al-Sharji, N. K. Al Rasbi, A. Macchioni, L. Zhou, W.-Y. Wong, P. R. Raithby, M. S. Khan, *Dyes Pigm.* **2022**, *203*, 110300; (c) R. Ilmi, D. Zhang, J. D. L. Dutra, N. Dege, L. Zhou, W.-Y. Wong, P. R. Raithby, M. S. Khan, *Org. Electron.* **2021**, *96*, 106216.

[2] (a) J. Sun, B. Song, Z. Ye, J. Yuan, *Inorg. Chem.* **2015**, *54*, 11660-11668; (b) J. Wu, Y. Xing, H. Wang, H. J. Liu, M. Yang, J. L. Yuan, *New J. Chem.* **2017**, *41*, 15187-15194; (c) V. Divya, V. Sankar, K. G. Raghu, M. L. P. Reddy, *Dalton Trans.* **2013**, *42*, 12317-12323; (d) J. Wu, Y. Xing, H. Wang, H. Liu, M. Yang, J. Yuan, *New J. Chem.* **2017**, *41*, 15187-15194.

[3] (a) R. Ilmi, M. S. Khan, Z. Li, L. Zhou, W.-Y. Wong, F. Marken, P. R. Raithby, *Inorg. Chem.* **2019**, *58*, 8316-8331; (b) S. Li, L. Zhou, H. Zhang, *Light: Science & Applications* **2022**, *11*, 177.

[4] S. Mund, S. Vaidyanathan, *J. Mater. Chem. C* **2022**, *10*, 7201-7215.

[5] J.-C. G. Bünzli, A.-S. Chauvin, H. K. Kim, E. Deiters, S. V. Eliseeva, *Coord. Chem. Rev.* **2010**, *254*, 2623-2633.

[6] N. M. Shavaleev, S. V. Eliseeva, R. Scopelliti, J.-C. G. Bünzli, *Chem. Eur. J.* **2009**, *15*, 10790-10802.

[7] M. S. Khan, R. Ilmi, W. Sun, J. D. L. Dutra, W. F. Oliveira, L. Zhou, W.-Y. Wong, P. R. Raithby, *J. Mater. Chem. C* **2020**, *8*, 5600-5612.

[8] (a) B. R. Judd, *Phys. Rev.* **1962**, *127*, 750-761; (b) G. S. Ofelt, *J. Chem. Phys.* **1962**, *37*, 511-520.

[9] P. P. Ferreira da Rosa, Y. Kitagawa, Y. Hasegawa, *Coord. Chem. Rev.* **2020**, *406*, 213153.

[10] (a) K. Miyata, Y. Hasegawa, Y. Kuramochi, T. Nakagawa, T. Yokoo, T. Kawai, *Eur. J. Inorg. Chem.* **2009**, *2009*, 4777-4785; (b) R. Ilmi, N. Hasan, J. Liu, D. Mara, R. Van Deun, K. Iftikhar, *J. Photochem. Photobiol., A* **2017**, *347*, 116-129.

[11] N. Hasan, K. Iftikhar, *J. Lumin.* **2020**, *223*, 117135.

[12] (a) R. Ilmi, W. Sun, J. D. L. Dutra, N. K. Al-Rasbi, L. Zhou, P.-C. Qian, W.-Y. Wong, P. R. Raithby, M. S. Khan, *J. Mater. Chem. C* **2020**, *8*, 9816-9827; (b) R. Ilmi, M. S. Khan, W. Sun, L. Zhou, W.-Y. Wong, P. R. Raithby, *J. Mater. Chem. C* **2019**, *7*, 13966-13975.

[13] (a) A. Wild, A. Winter, F. Schlütter, U. S. Schubert, *Chem. Soc. Rev.* **2011**, *40*, 1459-1511; (b) R. R. Panicker, A. Sivaramakrishna, *Coord. Chem. Rev.* **2022**, *459*, 214426.

[14] J. D. Dutra, T. D. Bispo, R. O. Freire, *J. Comput. Chem.* **2014**, *35*, 772-775.

[15] H.-B. Cheng, H.-Y. Zhang, Y. Liu, *J. Am. Chem. Soc.* **2013**, *135*, 10190-10193.

[16] C. Yang, J. Xu, Y. Zhang, Y. Li, J. Zheng, L. Liang, M. Lu, *J. Mater. Chem. C* **2013**, *1*, 4885-4901.

[17] A. Carlotto, L. Babetto, S. Carlotto, M. Miozzi, R. Seraglia, M. Casarin, G. Bottaro, M. Rancan, L. Armelao, *ChemPhotoChem* **2020**, *4*, 674-684.

[18] C. R. De Silva, J. R. Maeyer, A. Dawson, Z. Zheng, *Polyhedron* **2007**, *26*, 1229-1238.

[19] (a) M. Pinsky, D. Avnir, *Inorg. Chem.* **1998**, *37*, 5575-5582; (b) D. Casanova, M. Llunell, P. Alemany, S. Alvarez, *Chem. Eur. J.* **2005**, *11*, 1479-1494.

[20] D. Jacquemin, E. A. Perpète, I. Ciofini, C. Adamo, *J. Chem. Theory Comput.* **2010**, *6*, 1532-1537.

[21] R. L. Martin, *J. Chem. Phys.* **2003**, *118*, 4775-4777.

[22] S. I. Weissman, *J. Chem. Phys.* **1942**, *10*, 214-217.

[23] R. Ilmi, S. Anjum, A. Haque, M. S. Khan, *J. Photochem. Photobiol., A* **2019**, *383*, 111968.

[24] J. Wu, H. Liu, Y. Yang, H. Wang, M. Yang, *Opt. Mater.* **2018**, *77*, 170-177.

[25] (a) M. H. V. Werts, R. T. F. Jukes, J. W. Verhoeven, *Phys. Chem. Chem. Phys.* **2002**, *4*, 1542-1548; (b) Y. Hasegawa, M. Yamamuro, Y. Wada, N. Kanehisa, Y. Kai, S. Yanagida, *J. Phys. Chem A* **2003**, *107*, 1697-1702.

[26] N. M. Shavaleev, S. V. Eliseeva, R. Scopelliti, J.-C. G. Bünzli, *Inorg. Chem.* **2015**, *54*, 9166-9173.

[27] Z. Abbas, S. Dasari, M. J. Beltrán-Leiva, P. Cantero-López, D. Páez-Hernández, R. Arratia-Pérez, R. J. Butcher, A. K. Patra, *New J. Chem.* **2019**, *43*, 15139-15152.

[28] J. D. L. Dutra, N. B. D. Lima, R. O. Freire, A. M. Simas, *Sci. Rep.* **2015**, *5*, 13695.

[29] A. N. Carneiro Neto, E. E. S. Teotonio, G. F. de Sá, H. F. Brito, J. Legendziewicz, L. D. Carlos, M. C. F. C. Felinto, P. Gawryszewska, R. T. Moura, R. L. Longo, W. M. Faustino, O. L. Malta, in *Handbook on the Physics and Chemistry of Rare Earths, Vol. 56* (Eds.: J.-C. G. Bünzli, V. K. Pecharsky), Elsevier, **2019**, pp. 55-162.

[30] D. Jacquemin, E. A. Perpète, I. Ciofini, C. Adamo, *J Chem Theory Comput* **2010**, *6*, 1532-1537.

[31] (a) M. Uchida, C. Adachi, T. Koyama, Y. Taniguchi, *J Appl Phys* **1999**, *86*, 1680-1687; (b) S. Blumstengel, F. Meinardi, R. Tubino, M. Gurioli, M. Jandke, P. Strohriegl, *J. Chem.Phys.* **2001**, *115*, 3249-3255.

[32] J.-W. Kang, S.-H. Lee, H.-D. Park, W.-I. Jeong, K.-M. Yoo, Y.-S. Park, J.-J. Kim, *Appl. Phys. Lett.* **2007**, *90*, 223508.

[33] A. Kovalenko, L. O. Tcelykh, D. Koshelev, A. A. Vashchenko, D. M. Tsymbarenko, A. S. Goloveshkin, A. Aleksandrov, A. Burlov, V. V. Utochnikova, *Dalton Trans.* **2022**, *51*, 3833-3838.

[34] (a) B. Francis, M. M. Nolasco, P. Brandão, R. A. S. Ferreira, R. S. Carvalho, M. Cremona, L. D. Carlos, *Eur. J. Inorg. Chem.* **2020**, *2020*, 1260-1270; (b) S. Biju, L.-J. Xu, M. A. Hora Alves, R. O. Freire, Z.-N. Chen, *New J. Chem.* **2017**, *41*, 1687-1695; (c) J. Wang, C. Han, G. Xie, Y. Wei, Q. Xue, P. Yan, H. Xu, *Chem. Eur. J.* **2014**, *20*, 11137-11148; (d) S. Zhang, G. A. Turnbull, I. D. W. Samuel, *Org. Electron.* **2012**, *13*, 3091-3096; (e) H. Xu, K. Yin, W. Huang, *Synthetic Metals* **2010**, *160*, 2197-2202; (f) L. Zhou, H. Zhang, W. Shi, R. Deng, Z. Li, J. Yu, Z. Guo, *J Appl Phys* **2008**, *104*, 114507; (g) Z. Chen, F. Ding, F. Hao, M. Guan, Z. Bian, B. Ding, C. Huang, *New J. Chem.* **2010**, *34*, 487-494; (h) F. Liang, Q. Zhou,

Y. Cheng, L. Wang, D. Ma, X. Jing, F. Wang, *Chem. Mater.* **2003**, *15*, 1935-1937; (i) L. Huang, K.-Z. Wang, C.-H. Huang, F.-Y. Li, Y.-Y. Huang, *J. Mater. Chem.* **2001**, *11*, 790-793.

[35] B. Zhao, H. Zhang, Y. Miao, Z. Wang, L. Gao, H. Wang, Y. Hao, B. Xu, W. Li, *J. Mater. Chem. C* **2017**, *5*, 12182-12188.

[36] M. Pietraszkiewicz, M. Maciejczyk, I. D. W. Samuel, S. Zhang, *J. Mater. Chem. C* **2013**, *1*, 8028-8032.

[37] H. Xu, K. Yin, W. Huang, *Chem. Eur. J.* **2007**, *13*, 10281-10293.

[38] Y. Liu, Y. Wang, H. Guo, M. Zhu, C. Li, J. Peng, W. Zhu, Y. Cao, *J. Phys. Chem. C* **2011**, *115*, 4209-4216.

[39] H. Xu, K. Yin, W. Huang, *J. Phys. Chem. C* **2010**, *114*, 1674-1683.

[40] H. Xu, L.-H. Wang, X.-H. Zhu, K. Yin, G.-Y. Zhong, X.-Y. Hou, W. Huang, *J. Phys. Chem. B* **2006**, *110*, 3023-3029.

[41] I. J. Al-Busaidi, R. Ilmi, D. Zhang, J. D. L. Dutra, W. F. Oliveira, N. K. Al Rasbi, L. Zhou, W.-Y. Wong, P. R. Raithby, M. S. Khan, *Dyes Pigm.* **2022**, *197*, 109879.

[42] S. Wang, J. Zhang, Y. Hou, C. Du, Y. Wu, *J. Mater. Chem.* **2011**, *21*, 7559-7561.

[43] Y. Liu, J. Li, C. Li, J. Song, Y. Zhang, J. Peng, X. Wang, M. Zhu, Y. Cao, W. Zhu, *Chem. Phys. Lett.* **2007**, *433*, 331-334.

[44] Y. Ma, S. Liu, H. Yang, Y. Zeng, P. She, N. Zhu, C.-L. Ho, Q. Zhao, W. Huang, W.-Y. Wong, *Inorg. Chem.* **2017**, *56*, 2409-2416.